

# The ability of general circulation models to simulate tropical cyclones and their precursors over the North Atlantic main development region

Anne Sophie Daloz · Fabrice Chauvin ·  
Kevin Walsh · Sally Lavender · Deborah Abbs ·  
Frank Roux

Received: 24 May 2011 / Accepted: 9 January 2012 / Published online: 19 January 2012  
© Springer-Verlag 2012

**Abstract** The ability of General Circulation Models (GCMs) to generate Tropical Cyclones (TCs) over the North Atlantic Main Development Region (MDR; 10–20°N, 20–80°W; Goldenberg and Shapiro in *J Clim* 9:1169–1187, 1996) is examined through a subset of ocean–atmosphere coupled simulations from the World Climate Research Programme (WCRP) Coupled Model Intercomparison Project phase 3 (CMIP3) multimodel data set and a high-resolution (0.5°) Sea Surface Temperature (SST)-forced simulation from the Australian Conformal-Cubic Atmospheric Model GCM. The results are compared with National Center for Environmental Prediction (NCEP-2) and European Center for Medium Range Weather Forecasts Re-Analysis (ERA-40) reanalyses over a common period from 1980 to 1998. Important biases in the representation of the TC activity are encountered over the MDR. This study emphasizes the strong link in the GCMs between African Easterly Waves (AEWs) and TC activity in this region. However, the generation of AEWs is not a sufficient

condition alone for the models to produce TCs. Precipitation over the Sahel, especially rainfall over the Fouta Djallon highlands (cf. Fig. 1), is playing a role in the generation of TCs over the MDR. The influence of large-scale fields such as SST, vertical wind shear and tropospheric humidity on TC genesis is also examined. The ability of TC genesis indices, such as the Genesis Potential Index and the Convective Yearly Genesis Potential, to represent TC activity over the MDR in simulations at low to high spatial resolutions is analysed. These indices are found to be a reasonable method for comparing cyclogenesis in different models, even though other factors such as AEW activity should also be considered.

**Keywords** Tropical cyclone (TC) · African Easterly Wave (AEW) · General Circulation Model (GCM) · Precursor

## 1 Introduction

It has long been recognized that General Circulation Models (GCMs) are able to produce systems reminiscent of tropical cyclones (TCs) in the North Atlantic basin (Manabe et al. 1970; Bengtsson et al. 1982; Krishnamurti et al. 1989; Broccoli and Manabe 1990; Haarsma et al. 1993). African Easterly Waves (AEWs) are known to be connected to the occurrence of TCs in this region (Burpee 1974; Reed et al. 1977; Thompson et al. 1979; Landsea and Gray 1992). However, many GCMs fail to represent TC activity in the North Atlantic basin (Camargo et al. 2005; Royer and Chauvin 2009). A bias in the representation of AEW activity can at least partially explain this problem, but the lack of TC activity over the Atlantic basin and the North Atlantic Main Development Region (MDR) can have

---

A. S. Daloz (✉) · F. Chauvin  
Groupe de Modélisation Grande Echelle et Climat,  
CNRM-GAME, Météo-France, 42 avenue G. Coriolis,  
31057 Toulouse Cedex 1, France  
e-mail: anne-sophie.daloz@cnrm.meteo.fr

K. Walsh  
School of Earth Sciences, University of Melbourne,  
Melbourne, VIC, Australia

S. Lavender · D. Abbs  
CSIRO Atmospheric and Marine Research, Aspendale,  
VIC, Australia

F. Roux  
Laboratoire d'Aérodynamique, Université de Toulouse and Centre  
National de la Recherche Scientifique, Toulouse, France

other causes. The ability of models to capture the El Niño Southern Oscillation (ENSO) may greatly influence their ability to represent North Atlantic TC activity (Camargo et al. 2007) since ENSO changes the large-scale environmental factors that are known to strongly influence TC genesis (Gray 1968). In particular, the vertical shear of the horizontal wind in the troposphere is considered to be one of the major variables influencing cyclogenesis (Gray 1968), particularly over the Atlantic (Vecchi and Soden 2007).

In the Atlantic, the official hurricane season begins June 1 and ends November 30, although activity has been observed outside this time frame. Genesis locations vary during the hurricane season (Neumann et al. 1999) and three time periods can be distinguished based on these locations:

- Early-season (1 June–15 July), storms mostly originate in the western Caribbean Sea and the Gulf of Mexico, and are quite rare in the MDR.
- Mid-season (16 July–20 September), storms form mostly in the MDR.
- The late season (21 September–30 November) has a gradual decline in TC numbers over the whole region with genesis in the MDR declining more rapidly.

Genesis in the MDR peaks in the mid-season because sea surface temperatures (SSTs) are warm enough to sustain intense and long-lived convective activity associated with tropical waves that propagate off the African continent and over the eastern tropical Atlantic. The peak in TC activity over the MDR is also linked with a peak of AEW activity in the mid-season (Thorncroft and Hodges 2001; Hopsch et al. 2007). In this study, the eastern (western) tropical Atlantic is defined as the North Atlantic tropical basin east (west) of 60°W (Fig. 1).

During boreal summer, the atmospheric circulation over West Africa exhibits a strong monsoon flow, advecting moist air from the Gulf of Guinea and the nearby tropical Atlantic toward the interior of the continent. The West

African troposphere during the monsoon season is characterized by a mid-tropospheric zonal wind maximum (the African Easterly Jet—AEJ), which peaks at 600–700 hPa. Synoptic systems (AEWs), a well known feature of the summer West African climate, develop on the sides of this jet (Ruti and Dell'Aquila 2010). These propagating AEW disturbances have been studied for many years, particularly during GATE (Global Atmospheric Research Program's Atlantic Tropical Experiment, Reed et al. 1977), AMMA (African Monsoon Multidisciplinary Analyses, Redelsperger et al. 2006) and PREDICT (Pre-Depression Investigation of Cloud-System in the Tropics, Montgomery (2011)). Burpee (1972) was the first to suggest that horizontal and vertical shear of the mean zonal wind could induce barotropic and/or baroclinic instabilities and dynamic perturbations with characteristics similar to those of the AEWs. This has led to a number of other studies on AEWs (Burpee 1972; Thorncroft and Hoskins 1994; Chen et al. 2006; Hsieh and Cook 2007). AEW disturbances are located at a mean latitude of 12°N over land and typically have periods of 3–5 days, wavelengths of 2,000–4,000 km, and a westward mean propagation speed of about 6°–7° per day (7–9 m/s) (Reed et al. 1977). The link between tropical disturbances over West Africa and Atlantic TCs was suggested by Carlson (1969), and this is still an important subject in more recent scientific investigations (e.g. Reed et al. 1988; Thorncroft and Hodges 2001; Hopsch et al. 2007; Caron et al. 2010; Arnault and Roux 2011).

The association between Sahelian rainfall and hurricane activity was first investigated by Gray (1990). Landsea and Gray (1992) generalized this study and proposed two physical mechanisms which may explain the link between Sahelian rainfall and intense TC activity. They established that during dry (wet) years, there were less (more) intense TCs. This year-to-year co-variation could be related to two different mechanisms. First, the change in the atmospheric upper-level circulation over the MDR during wet (dry) years leads to a reduced (enhanced) horizontal wind shear which is favourable (unfavourable) to TC genesis. The second hypothesis hints at a possible relation between Sahelian rainfall and the interannual variations of AEWs amplitude. During dry (wet) years over Sahel, this amplitude decreases (increases) leading to a reduced (enhanced) genesis of TCs. Landsea and Gray (1992) based their study on data from the time period 1949–1990. More recently, Klotzbach and Gray (2004) showed that the relationship broke down in the mid 1990's for as yet unexplained reasons. Changes in the strength of the relationship have been shown to vary with time (Fink et al. 2010) and are also influenced by changes in environmental factors such as SST and vertical wind shear.

To diagnose the number of TCs in GCMs, two techniques have generally been employed. The first one



Fig. 1 Map of West Africa. Source <http://www.junglephotos.com/>

consists in locating and tracking “pseudo-TCs” (Haarsma et al. 1993; Bengtsson et al. 1996; Walsh and Watterson 1997; Sugi et al. 2002; McDonald et al. 2005; Chauvin et al. 2006; Oouchi et al. 2006; Bengtsson et al. 2007; Walsh et al. 2007). GCM resolutions are too coarse to simulate realistic TCs and instead reproduce systems reminiscent of TCs, but with slightly different characteristics. For example, they cannot reproduce the eye structure of TCs. The second technique provides an estimate of TC activity through the use of genesis parameters depending on seasonal mean values of large-scale fields. Empirically developed cyclogenesis indices reproduce the distribution of TCs with some accuracy for the present climate. The Seasonal Genesis Parameter (SGP) was developed by Gray (1975) and was used to assess climatological genesis. More recently, Royer et al. (1998) proposed the Convective SGP (CSGP) which retains some of the parameters of the SGP, but replaces those considered as unreliable in future climate conditions. In the SGP, the thermal effect of ocean is taken into account through the integration of SST above 26°C down to 60 m depth, as this temperature is typically the threshold in the current climate for the development of tropical deep convection (e.g. Sud et al. 1999). Royer et al. (1998) showed that, in the context of global warming, the thermal effect of ocean and the threshold of 26°C should be replaced by a more physical process, such as convective precipitation which leads to an index named the CYGP (Convective Yearly Genesis Potential). Instead of considering a SST threshold, the thermodynamic potential in the CYGP is defined through the derivation of the seasonal mean convective precipitation of the model. The underlying hypothesis is that the convective precipitation in the model integrates the atmospheric response to changes not only in SST, but also in static stability and tropospheric humidity. Another index, the Genesis Potential Index (GPI) was proposed by Emanuel and Nolan (2004). The main difference between the SGP and the GPI also comes from the thermodynamic potential. GPI uses potential intensity (Bister and Emanuel 1998), which depends on the air–sea thermodynamic disequilibrium and the difference between the SST and the temperature at the level of neutral buoyancy for an adiabatically lifted boundary layer parcel. GPI uses the near-surface ocean thermal energy and the vertical gradient of the equivalent potential temperature between the surface and 500 hPa.

Several ocean–atmosphere coupled model integrations have been performed for the the World Climate Research Programme (WCRP) Coupled Model Intercomparison Project phase 3 (CMIP3) and a subset of these have been analysed in the TC Model Intercomparison Project (TC-MIP, Walsh et al. 2010). The TC-MIP project aims to compare and analyze models performances in simulating TCs and to investigate the reasons for differences between models. The

TC-MIP results analyzed here are from coupled ocean–atmosphere simulations of the present climate, with spatial resolutions varying from  $1^\circ \times 1^\circ$  to  $2.8^\circ \times 2.8^\circ$ . A high-resolution ( $0.5^\circ$ ) bias-corrected SST forced simulation from the CSIRO Conformal Cubic Atmospheric Model (CCAM; McGregor and Dix 2001) is also analysed. The model data have been compared with the NCEP-2 and ERA-40 reanalyses over a common time period (1980–1998).

In the next section the datasets and tracking methodology are described. The ability of the GCMs to simulate the TC activity over the MDR is discussed in Sect. 3. In Sect. 4, precursors and factors influencing TC genesis such as AEW activity, Sahelian rainfall or tropospheric humidity are examined. Finally, the ability of tropical cyclogenesis indices to represent TC activity over the MDR is discussed in Sect. 5. Summary and conclusions are given in Sect. 6.

## 2 Datasets and methodology

### 2.1 Observations and reanalysis

#### 2.1.1 Global precipitation

The Global Precipitation Climatology Project (GPCP) (version 2.1; daily;  $1^\circ$  longitude by  $1^\circ$  latitude grid) daily precipitation is produced at the NASA Goddard Space Flight Center. Data from rain gauges, satellite geostationary and low-orbit infrared, passive microwave, and sounding observations have been merged to estimate daily rainfall. The different methods employed for the construction of this dataset are detailed in Huffman et al. (2001).

#### 2.1.2 NCEP-2 reanalysis

The National Centers for Environmental Prediction (NCEP)—National Center for Atmospheric Research (NCAR) reanalysis is a retrospective (since 1948) record of global analyses of atmospheric fields. The NCEP-2 reanalysis is an improved version including some corrections along with updated parameterizations of physical processes (Kanamitsu et al. 2002). The daily NCEP-2 reanalysis has a horizontal resolution of  $1.875^\circ \times 1.875^\circ$  at 28 levels unevenly distributed from the surface to 3 hPa. Meridional wind and total precipitation were used from this dataset.

#### 2.1.3 ERA-40 reanalysis

European Centre for Medium Range Weather Forecasts (ECMWF) Re-Analysis (ERA-40) is a 44-year (1958–2001) integration product (daily and monthly,  $1.12^\circ \times 1.12^\circ$  horizontal resolution) developed by ECMWF. This dataset is obtained through a global spectral model with T159L60.

More details can be found in Uppala et al. (2005). Meridional wind and total precipitation were used from this dataset.

## 2.2 TC-MIP and CCAM simulations

### 2.2.1 TC-MIP

The simulations analyzed in this study are a subset of model outputs from CMIP-3 (Meehl et al. 2007) as used in the TC-MIP (Walsh et al. 2010) with some common metrics related to TC formation. Coupled ocean–atmosphere models simulate the global climate during the 20th century, but we will focus here on July–August–September of the period 1980–1998 over the Atlantic Ocean and West Africa (hereafter referred to as JAS 1980–1998). The models have horizontal resolutions from  $1^\circ \times 1^\circ$  to  $5^\circ \times 4^\circ$ . While none of these models has a resolution suitable for the generation and maintenance of realistic TCs, it is nevertheless possible to compare their large-scale environmental characteristics and the simulated TC-like vortices. This study was restricted to the ten models with the highest resolution ( $1^\circ \times 1^\circ$  to  $2.8^\circ \times 2.8^\circ$ ) presented in Table 1.

### 2.2.2 CCAM

CCAM is the CSIRO (Australian Commonwealth Scientific and Industrial Research Organisation) Conformal-Cubic

Atmospheric Model described by McGregor and Dix (2001). A simulation over 1979–1998 with a spatial resolution of  $0.5^\circ$  was produced. The model is forced with bias-corrected SSTs. The bias is calculated for each seasonal month by removing climatological observed SSTs to the SST climatology produced by a low resolution coupled version of CCAM. Then, the bias is removed from the initial interannual low-varying SST coupled field and prescribed to high resolution version of CCAM. As a result, GCM-dependent interannual variability is retained while monthly climatological biases are removed. No atmospheric nudging is used in this CCAM simulation. Nineteen years of the CCAM simulation were available (1980–1998) when this study was conducted, explaining the choice of time period.

## 2.3 TC tracking

### 2.3.1 IBTrACS

The International Best Track Archive for Climate Stewardship (IBTrACS) is a global dataset containing information on all documented TCs compiled and archived by different agencies around the world generated by the NOAA (United States of America National Oceanic and Atmospheric Administration) Climatic Data Center (NCDC). The methods used to combine the different datasets into a centralized archive are detailed in Knapp et al. (2010).

**Table 1** Characteristics of the selected TCMIP and CCAM simulations, and NCEP-2 and ERA-40 reanalyses

Dataset	Institution	Spatial resolution in degrees	Main difference between simulations of the same model
CNRM	CNRM—Centre National de Recherches Meteorologiques (France)	$2.8 \times 2.8$	Only one simulation
CSIRO0	CSIRO—Commonwealth Scientific and Research Organization (Australia)	$1.9 \times 1.9$	CSIRO0 has been upgraded in all part of CSIRO1. In particular, in the ocean model, CSIRO1 includes spatial varying eddy transfer coefficient and Kraus-Turner mixed layer scheme (CAWCR Technical Report N21)
CSIRO1		$1.9 \times 1.9$	
GFDL0	GFDL—Geophysical Fluid Dynamics Laboratory (USA)	$2.5 \times 2.0$	GFDL0 uses a B-grid finite difference dynamical core and GFDL1 a finite-volume dynamical core (Delworth et al. 2006)
GFDL1		$2.5 \times 2.0$	
IAP	IAP—Institute of Atmospheric Physics (China)	$2.8 \times 2.8$	Only one simulation
MIRO0	University of Tokyo, National Institute for environmental studies and JAMSTEC, Japan Agency for Marine Earth Science and Technology (Japan)	$1.1 \times 1.1$	The difference between the two simulations is the spatial resolution
MIRO1		$2.8 \times 2.8$	
MPI	MPI—Max Planck Institute (Germany)	$1.8 \times 1.8$	Only one simulation
MRI	MRI—Meteorological Research Institute (Japan)	$2.8 \times 2.8$	Only one simulation
CCAM	CCAM—Conformal Cubic Atmospheric Model, CSIRO	$0.5 \times 0.5$	Only one simulation
NCEP-2	NCEP—National Center for Environmental Prediction (USA)	$1.875 \times 1.875$	Reanalyses
ERA-40	ECMWF—European Center for Medium Range Forecasts (England)	$1.12 \times 1.12$	Reanalyses

### 2.3.2 Climate models

To assess TC activity, the use of an automated procedure to track individual storms proved to produce the best result. The tracking method proposed by Walsh et al. (2004) has been chosen here, but with the objectively derived resolution-dependent wind speed threshold criterion from Walsh et al. (2007), so as to allow comparison of simulations using different spatial resolutions. Taking into account that the maximum wind speed in a simulation depends on its resolution, Walsh et al. (2007) defined an empirical relationship between resolution and wind speed threshold which is to be used in tracking algorithms.

The criteria for detecting TCs in the model data are:

1. The maximum 10-m wind speed simulated in the storm must be larger than a resolution-dependent threshold corresponding to the observed  $17 \text{ m s}^{-1}$  tropical storm limit. From an analytical wind profile model and two-dimensional observed wind analysis, Walsh et al. (2007) showed that this threshold varies roughly linearly with resolution. Hence, the wind speed threshold is corrected using an adjustment factor related to the spatial resolution (see Table 2). A lower threshold was employed for the high-resolution CCAM results to give a better estimate of the geographical pattern of formation than typically generated by the other models. This becomes particularly important when examining the TC formation generated by this model in the MDR, as shown in Sect. 3.
2. Relative vorticity must be higher than  $10^{-5} \text{ s}^{-1}$ .
3. A closed pressure minimum must exist within a distance from a point satisfying (2), in order to verify correlation between vorticity maximum and pressure minimum. The location of the pressure minimum is then taken as the storm center. This distance depends on the horizontal resolution of the models. Based on some radius tests, the distance used was 1,000 km for the CMIP-3 models and 250 km for CCAM.
4. The total tropospheric temperature anomaly must be greater than zero. This anomaly is calculated by summing differences at 700, 500 and 300 hPa between the temperature around center of the storm and the mean value at each level in a domain of 1,200 km east, west and 400 km north, south of the storm center.
5. The temperature anomaly at the storm center must be larger at 300 hPa than at 850 hPa.
6. The mean tangential wind in a domain of  $800 \times 800 \text{ km}$  around the storm center must be greater at 850 hPa than at 300 hPa.

**Table 2** Numbers of detected TC occurrences globally (2nd column), in the MDR (3rd column) and associated wind speed thresholds (3rd column) for TCMIP and CCAM models, and for IBTrACS, over the time period JAS 1980–1998

Dataset	Occurrences detected globally	Occurrences detected over the MDR	Wind speed threshold ( $\text{m s}^{-1}$ )
cnrm	5,015	0	10.5
iap	1,610	0	10.5
mri	6,500	0	10.5
ccam	9,444	12	11.5
gfdl0	6,406	35	12
csiro0	14,172	61	13
mpi	11,743	87	10.5
csiro1	11,881	120	13
miro1	5,294	215	10.5
miro0	4,052	253	14.5
gfdl1	15,568	408	12
Ibtracs	25,613	933	17

### 2.4 Factors influencing TC activity over the MDR

The variables analysed to examine which factors are influencing TC formation in the models are described here. AEWs are known to influence tropical cyclogenesis over the Atlantic and in the MDR (Landsea 1993; Thorncroft and Hodges 2001; Hopsch et al. 2007, 2010; Arnault and Roux 2011). For each model, daily fields of meridional wind at 850 hPa were analysed to take into account AEW propagation. To evaluate the possible correlation between Sahelian rainfall and TC activity in models and reanalyses, as shown by Landsea and Gray (1992), mean precipitation values were analysed. Other large-scale fields (e.g. vertical wind shear, SST and mid-level humidity) were examined as they are known, among others, to influence TC genesis (Gray 1975). Their influence is known to vary among different basins. In the North Atlantic basin, Goldenberg and Shapiro (1996) showed that the vertical wind shear may be one of the most important features. Reduced wind shear is associated with increased activity while stronger wind shear with decreased activity. They also showed that most of the fluctuations in wind shear are associated to SST and rainfall variations. Garner et al. (2009) also noted the importance of the SST by showing that the vertical wind shear is largely determined by gradients of SST both locally over the Atlantic and remotely from the Indo-Pacific basin. Sall et al. (2006) and Arnault and Roux (2011) showed that mid-level humidity over the African coast is an important factor to understand why some waves develop into TCs while others do not. Recent studies (Hopsch et al. 2010 and Braun 2010) suggest that mid- to upper level humidity over the African coast and the Atlantic Ocean influence cyclogenesis. Hopsch

et al. (2010) showed that both developing and non-developing waves present moist low-level layers. However, from mid- to upper levels, developing waves present higher relative humidity values compared to non-developing waves. They suggest that this difference could be due to the negative influence of mid-level advection of dry air associated with the Saharan Air Layer (Dunion and Velden (2004).

## 2.5 Tropical cyclogenesis indices

Two techniques have been widely used to diagnose the number of TCs in GCMs. The first technique presented in Sect. 2 and used in Sects. 3 and 4, consists of using an automatic procedure to track individual storms using several criteria. The second technique estimates the possibility of TC genesis, usually in low resolution models, based on environmental fields known to have an influence on TC genesis. Here, we consider two indices: CYGP (Royer et al. 1998) and GPI (Emanuel and Nolan 2004).

For CYGP, the selected fields are the vertical wind shear ( $V_{\text{shear}}$ ) between the upper (200 hPa) and lower (850 hPa) troposphere,  $\varphi_r$  the relative vorticity at 850 hPa and  $P_c$  an estimate of convective precipitation exceeding a calibrated threshold depending on the total convective precipitation in the GCM (see Royer et al. 1998):

$$\text{CYGP} = k f (\varphi_r f / |f| + 5) (|V_{\text{shear}}| + 3)^{-1} P_c$$

where  $f$  is the Coriolis parameter and  $k$  is a calibration factor which assumes that the mean global TC genesis is 84 per year.

For GPI, the selected fields are the vertical wind shear  $V_{\text{shear}}$  between the upper (200 hPa) and lower (850 hPa) troposphere,  $\varphi_a$  the absolute vorticity,  $H$  the relative humidity at 700 hPa and  $V_{\text{pot}}$  the potential intensity as defined in Bister and Emanuel (1998):

$$\text{GPI} = |10^5 \varphi_a|^{3/2} (H/50)^3 (V_{\text{pot}}/70)^3 (1 + 0.1 V_{\text{shear}})^{-2}$$

These indices are representative of environmental conditions favourable to TC genesis and not of the real count of TCs (Royer et al. 1998; McDonald et al. 2005; Chauvin et al. 2006). Nevertheless, they provide a method for comparing models and their ability to produce TCs. Here, for all models, CYGP and GPI are compared with TC genesis numbers deduced from the tracking method for JAS 1980–1998. Both indices are corrected with a factor depending on the different spatial resolutions of the models.

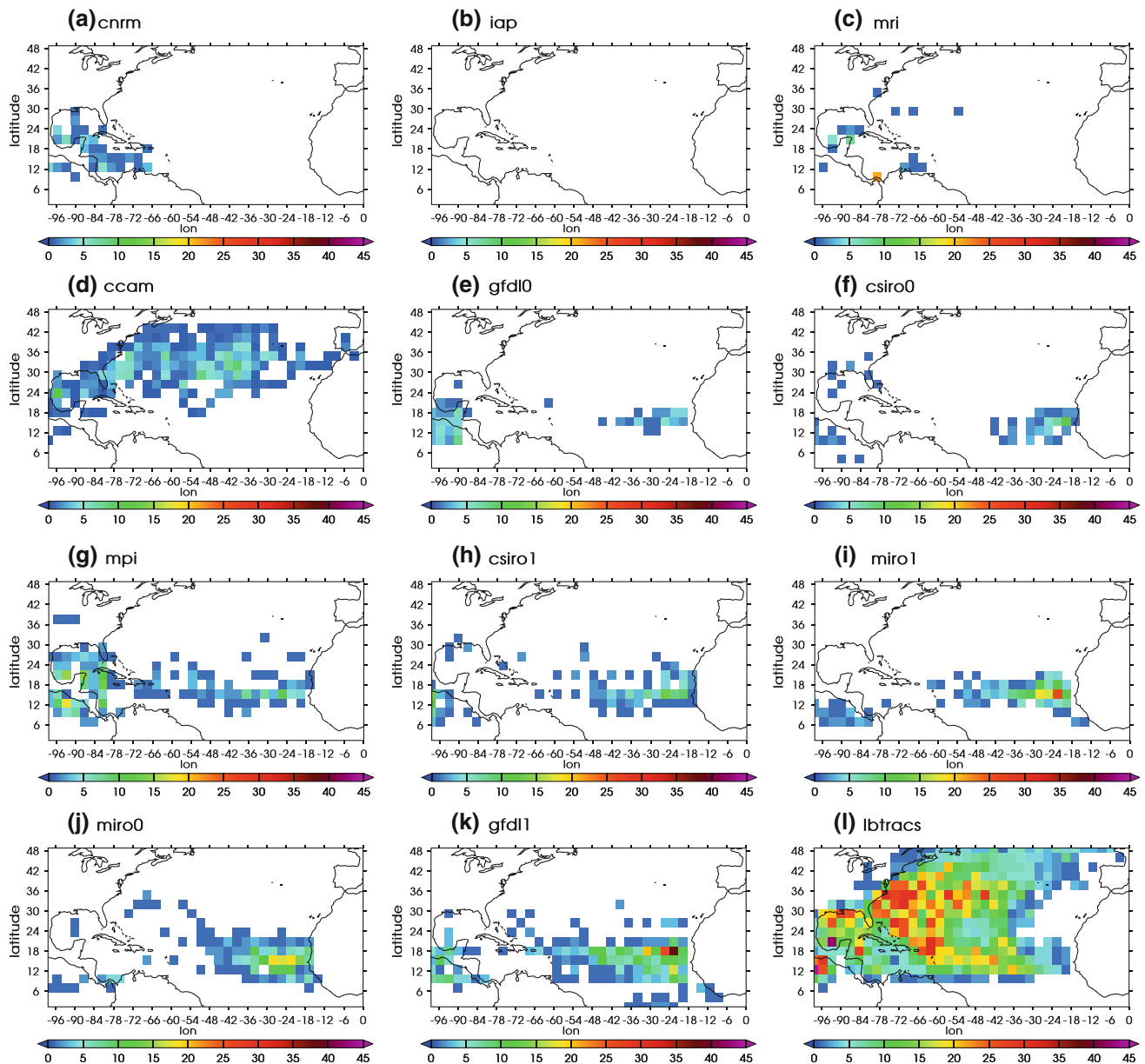
## 3 Observed and simulated TCs in the North Atlantic basin

Figure 2 presents the density of detected TC occurrences for the TC-MIP and CCAM models, and from IBTrACS

for JAS 1980–1998 over the North Atlantic basin. In Fig. 2, the simulations are sorted in accordance with their number of TC occurrences detected in the MDR (Table 2). This classification will be used throughout this paper. Although this study focuses on the MDR, it is interesting to first verify the ability of the GCMs to represent the North Atlantic TC activity as a whole. The density of TC occurrence for the different models (Fig. 2a–k) is highly variable and generally too low over the whole North Atlantic, including the MDR. It is clear from the large spread of the simulations that, even when corrected for their different resolutions by the use of a resolution-dependent wind speed threshold, models have problems in producing TCs over the Atlantic. Even those simulations that simulate TC activity largely underestimate its amplitude and do not correctly reproduce its geographic distribution in comparison with observations (Fig. 2l). The bias in localization is especially visible for CCAM which produces TCs only in the northern part of the Gulf of Mexico and the subtropical regions of the Atlantic. In fact, CCAM is the only model to produce significant activity over western Atlantic subtropics, clearly highlighting the geographical variation in the formation pattern analyzed in these results. However, the TC activity in CCAM is concentrated in this region which is not realistic compared to IBTrACS. This point will be investigated further later in this paper.

Seven models (CSIRO0, MIRO0, GFDL0, GFDL1, MIRO1, GFDL1 and MPI) reproduce TC activity in the MDR, even though they all underestimate it in comparison with IBTrACS. This TC activity is generally located too far east, close to the West African coast while IBTrACS shows a maximum density near the French Antilles. Table 2 summarises the number of TC occurrences detected globally (left column) and in the MDR (central column) from TC-MIP and CCAM simulations, and from IBTrACS. The right column shows the wind speed threshold used for each simulation, depending on its horizontal resolution. Table 2 clearly shows there is no link between detected global TC activity and MDR activity. For example, in CCAM the fraction of the total global number of TCs that form in the MDR region is small. The twelve occurrences of TCs simulated in the MDR in CCAM are the result of TCs recurring from the Gulf of Mexico or the western tropical Atlantic rather than forming in this region. Thus even with a low wind-speed threshold for its resolution, CCAM fails to generate storms in the MDR. However, CCAM TC formation is more frequent in the subtropics.

The MIRO0 model has one of the lowest rates of global TC activity, but one of the highest rates in the MDR. It can be noticed that MIRO1, with a coarser resolution than MIRO0, simulates more TCs globally,



**Fig. 2** Density of TCs detected over JAS 1980–1998 over the North Atlantic basin in : **a** CNRM, **b** IAP, **c** MRI, **d** CCAM, **e** GFDL0, **f** CSIRO0, **g** MPI, **h** CSIRO1, **i** MIRO1, **j** MIRO0, **k** GFDL1 and **l** IBTrACS

but has fewer TCs in the MDR. The GFDL models show a large spread in their results. Both globally and in the MDR region, GFDL0 largely underestimates TCs in comparison with GFDL1. For CSIRO simulations, it is interesting to note that CSIRO0 has more TCs than CSIRO1 globally, but CSIRO1 has more TC activity in the MDR. Compared with the actual number of TC occurrences in IBTrACS, all models are found to underestimate TC activity, globally by a factor of 1.5–15, and in the MDR by a factor of 2–10 for models which simulate TCs there.

#### 4 Relationship between TCs in the MDR, AEW activity and large-scale processes

In order to assess the models abilities in producing TC activity the different environmental features described in Sect. 2 will be addressed, as well as how they are reproduced by the models. These results are compared with NCEP-2 and ERA-40 reanalyses.

Figure 3 shows the 3–5 day bandpass filtered meridional wind variance at 850 hPa, averaged over the time period JAS 1980–1998 for the TCMIP, CCAM and reanalyses

over the western part of the African continent and Atlantic Ocean (10°S–30°N, 60°W–40°E). A 3–5 day bandpass filter (Fyfe 1999) has been applied to the meridional wind variance in order to isolate the AEW time-period. High values of filtered meridional wind variance indicate strong AEW activity. The range of values for ERA-40 in JAS 1980–1998 is similar to that obtained by Ruti and Dell’Aquila (2010) for the same reanalysis with a similar technique over 1961–2000. NCEP-2 shows a lower activity than ERA-40, which may be partially attributed to a coarser resolution. It is clear from Fig. 3 that most of TCMIP and CCAM simulations produce AEW activity with a maximum located close to the coastal maximum of the reanalyses (20°N, 20°W). Hence Fig. 3 and Table 3 confirm that a condition for the models to produce TCs in the MDR seems to be the ability to represent AEW activity. However, GFDL1 shows that this is not the only important condition.

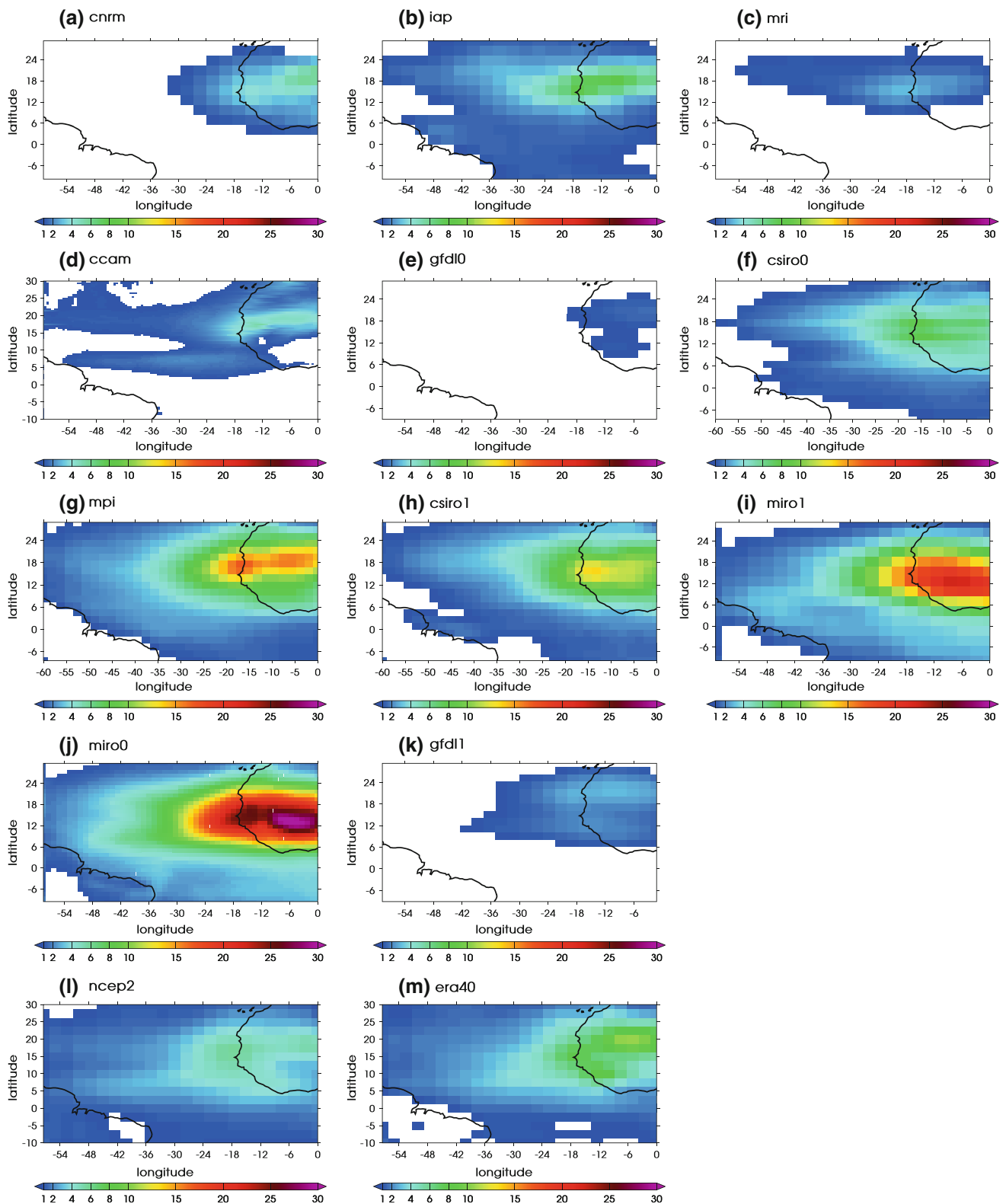
The mean precipitation for JAS 1980–1998 in the models, reanalyses and GPCP observations are shown in Fig. 4. Both reanalyses show realistic, although slightly overestimated, distribution of rainfall over West Africa and the tropical Atlantic compared to GPCP. In NCEP-2 the Intertropical Convergence Zone (ITCZ) over the central Atlantic has a southernmost location and a westernmost extension located at a more southwest location than in GPCP. Some models show a precipitation maximum located along the West African coast (near 8°N, 15°W), with values ranging from 6 mm day<sup>-1</sup> for IAP to 17 mm day<sup>-1</sup> for MIRO0 and MIRO1. However, some models (IAP, CSIRO0 and CCAM) are unable to reproduce this rainfall maximum, while MRI largely underestimates its amplitude and the maximum is located too south in CNRM. The reanalyses also show this maximum but with higher amplitudes of 19 mm day<sup>-1</sup> in NCEP-2 and GPCP and 25 mm day<sup>-1</sup> in ERA-40. All models also display a large area of relatively heavy precipitation, with values smaller than the maximum over the West African coast, related to the ITCZ between 5 and 20°N during boreal summer. This maximum is highly variable between the models, with maximum amplitudes from 5 mm day<sup>-1</sup> for IAP to 15 mm day<sup>-1</sup> for GFDL0, GFDL1, MIRO0, MIRO1 and CSIRO1. In this region, both reanalyses and GPCP show a mean rate of about 15 mm day<sup>-1</sup>. Apart from CNRM, MRI, CSIRO0, IAP and CCAM, the models are able to correctly represent the mean JAS 1980–1998 precipitation. CNRM, MRI and IAP are clearly underestimating the belt of precipitation. CSIRO0 shows higher amplitude compared with these three models, but it is still lower than the other models, reanalyses and observations. Finally, CCAM gives realistic amplitude over the ocean, but an important dry bias exists over the continent.

Table 3 summarises the AEW activity averaged over the West African continent (10–20°N, 15°W–10°E). In terms of amplitude of averaged activity, the results for the different models are very varied ranging from 0.77 m<sup>2</sup> s<sup>-2</sup> for GFDL0 to 22.08 m<sup>2</sup> s<sup>-2</sup> for MIRO0. ERA-40 and NCEP-2 have values of 5.9 and 3.7 m<sup>2</sup> s<sup>-2</sup> respectively. Among the models, a group of four (MIRO1, CSIRO1, MPI and MIRO0) show AEW activity higher than in ERA-40 and NCEP-2. MIRO0 (20.9 m<sup>2</sup> s<sup>-2</sup>) and MIRO1 (15.9 m<sup>2</sup> s<sup>-2</sup>) are particularly active compared with other models. It is interesting to note that three of the models which overestimate AEW activity (MIRO1, CSIRO1 and MIRO0) are among those which produce the highest TC activity over the MDR (Table 2). The reason why GFDL1 has a high TC count (Table 2) in spite of low AEW activity (Table 3) will be discussed in the following sections.

In Table 3, the mean Sahelian rainfall for the JAS season is also summarised. Precipitation has been averaged for JAS 1980–1998, over 10–20°N and 15°W–10°E. In both NCEP-2 and ERA-40 reanalyses, the mean rate is 1.7 mm day<sup>-1</sup> and in GPCP (not shown), the mean rate of precipitation over this region is 3 mm day<sup>-1</sup>. The rainfall averages for the simulations range from 1.5 mm day<sup>-1</sup> for CCAM to 5.3 mm day<sup>-1</sup> for GFDL0. MRI, IAP, CSIRO0 and CCAM all underestimate the total rainfall (cf. Fig. 4) but have a mean Sahelian rainfall close to those from NCEP-2 and ERA-40, however they are below the value from GPCP. CNRM, MPI, CSIRO1, MIRO1 and MIRO0 overestimate Sahelian rainfall in comparison with NCEP-2 or ERA-40, but are close to GPCP. GFDL0 and GFDL1 overestimate Sahelian rainfall in comparison with both reanalysis and GPCP. This high rainfall rate could explain the relatively strong TC activity over the MDR for GFDL1 in spite of a low AEW activity. On the other hand, GFDL0 has AEW activity 1.7 times lower than GFDL1, which cannot be balanced by a higher rainfall rate. Table 3 shows that a direct relationship between TC activity in the MDR (Table 2) and Sahelian rainfall (Table 3) is difficult to identify in the models.

The MDR and the Foutta Djallon (FD) rainfall (8–12°N; 15°E–5°W) for JAS 1980–1998 (Table 3) can also be compared with TC activity. As the number of TC occurrences increases in the different models, one could expect the MDR rainfall to show the same tendency considering that precipitation is a good indicator for convection. A region where convection develops is likely to be more favourable for the development of TC activity. However, there is no related increase in precipitation which indicates that there is no direct link between TC activity and precipitation over the MDR. Unlike MDR rainfall, FD rainfall does appear to be related with TC activity in the models.





**Fig. 3** As in Fig. 2, except for 3–5 day bandpass filtered variance of the meridional wind ( $\text{m}^2 \text{s}^{-2}$ ) at 850 hPa, and **l** for NCEP2, **m** for ERA40

Moderate to high AEW activity combined with moderate to high FD rainfall seems to lead to TC genesis. Globally, TC numbers increase with FD rainfall.

Table 3 also shows specific humidity at 600 hPa averaged for JAS 1980–1998, over the eastern tropical Atlantic ( $5^\circ\text{--}15^\circ\text{N}$ ,  $15^\circ\text{--}30^\circ\text{W}$ ), a region important for the

**Table 3** AEW activity ( $\text{m}^2 \text{s}^{-2}$ ; 10 N–20 N 15 W–10E), Sahelian rainfall ( $\text{mm day}^{-1}$ ; 10 N–20 N 15 W–10E), SST ( $^{\circ}\text{C}$ ; 10 N–20 N 80 W–20 W), vertical wind shear ( $\text{m s}^{-1}$ ; 10 N–20 N 80 W–20 W), MDR rainfall ( $\text{mm day}^{-1}$ ; 10 N–20 N 80 W–20 W), Fouta Djallon

rainfall ( $\text{mm day}^{-1}$ ; 8 N–12 N 15 W–5 W) and specific humidity at 600 hPa ( $\text{g kg}^{-1}$ ; 5 N–15 N, 15 W–10E) for JAS 1980–1998 from TCMIP and CCAM simulations, ERA-40 and NCEP-2 reanalyses

Dataset	AEW activity	Sahelian rainfall	SST MDR	Shear MDR	Rainfall MDR	Rainfall FD	HUM
cnrm	3.6	2.3	25.0	12.2	2.5	4.4	4.6
iap	4.4	1.6	26.0	18.8	1.0	4.9	4.2
mri	1.4	1.7	26.7	17.3	0.9	7.8	4.1
ccam	2.1	1.5	27.1	10.5	3.2	6.7	4.7
gfdl0	1.0	5.3	26.5	12.6	3.1	13.7	4.7
csiro0	5.1	1.8	25.0	14.9	1.1	6.9	3.8
mpi	9.6	2.8	27.7	8.5	3.1	9.6	5.6
csiro1	9.0	3.3	28.2	12.2	2.8	12.5	5.7
miro1	15.9	3	26.1	14.0	1.8	15.0	4.5
miro0	20.9	3	26.0	15.2	2.0	13.3	4.0
gfdl1	1.7	4.6	27.1	10.5	4.5	13.8	5.1
ncep2	3.7	1.7	27.5	11.1	2.4	13.5	4.0
era40	5.9	1.7	27.4	11.1	4.5	16.8	4.6

development of AEWs (e.g. Arnault and Roux 2011). This level corresponds to strong vertical humidity gradients and discriminates well between dry and humid air masses (Sall et al. 2006) which may conduce or not to TC development. Mean values of specific humidity for the reanalyses are  $4 \text{ g kg}^{-1}$  for NCEP-2 and  $4.6 \text{ g kg}^{-1}$  for ERA-40. For the simulations, the mean specific humidity ranges from less than  $4 \text{ g kg}^{-1}$  for CSIRO0 to more than  $5 \text{ g kg}^{-1}$  for MPI, CSIRO1 and GFDL1. Four (MIRO0, MIRO1, MPI, CSIRO1) of the 7 models that simulate TCs in the MDR have high AEW activity combined with moderate to high specific humidity. This result is consistent with previous studies (e.g. Sall et al. 2006; Hopsch et al. 2010 and Arnault and Roux 2011) which showed that a combination of AEW activity and high humidity over the ocean is a favourable environment for the development of TCs.

Mean SSTs for the reanalyses are  $27.6^{\circ}\text{C}$  for NCEP-2 and  $26.5^{\circ}\text{C}$  for ERA-40 (Table 3). For the models, the mean SST ranges from  $25.1^{\circ}\text{C}$  for CSIRO0 to  $28.2^{\circ}\text{C}$  for CSIRO1. GFDL1, CSIRO1, MPI and CCAM have warm SST (above  $27^{\circ}\text{C}$ ) which is favourable for cyclogenesis. On the other hand, CNRM and CSIRO0 have slightly colder SST values, close to  $25^{\circ}\text{C}$ . Both reanalyses show a vertical wind shear (calculated as the mean wind difference between 850 and 200 hPa) over the MDR of  $11.1 \text{ m/s}$  (Table 3). For the models, the vertical wind shear ranges from  $8.5 \text{ ms}^{-1}$  for CSIRO0 to  $18.8 \text{ ms}^{-1}$  for IAP.

Figure 5 is a scatter plot of AEW activity and Sahelian rainfall from the models, using the values from Table 3. In Figs. 5, 6, 7, 8, 9, NCEP-2 and ERA-40 results have also been added in order to have an idea of the behavior of observations relatively to these variables. ERA-40 and

NCEP-2 present very similar positions in the scatter plot (cf. Fig. 5) due to their low AEW activity and low Sahelian rainfall. Both of the reanalysis are located close to most of the models not producing TCs. Indeed, the models can be split into three different groups depending on their simulation of Sahelian rainfall and AEWs:

1. CCAM, MRI, IAP, CNRM and CSIRO0 have low AEW activity and low Sahelian rainfall. These models, with the exception of CSIRO0, do not produce TCs in the MDR.
2. MPI, CSIRO1, MIRO1 and MIRO0, have high AEW activity and moderate Sahelian rainfall. These models all simulate TCs in the MDR.
3. GFDL0 and GFDL1 have low AEW activity and high Sahelian rainfall and both simulate TCs in the MDR.

These results suggest that, for some models, TC activity over the MDR may be influenced by a combination of Sahelian rainfall and AEW activity. Models not producing TCs show both low Sahelian rainfall and AEW activity. On the other hand, models producing TCs present high Sahelian rainfall or high AEW activity, or both. From these results, the combination of AEW activity and Sahelian rainfall appears to be a good predictor of TC activity over the MDR.

Figure 6 is similar to Fig. 5 but showing MDR rainfall instead of Sahelian rainfall using the values in Table 3. ERA-40 and NCEP-2 show very different location on the scatter plot due to their difference in MDR rainfall. ERA-40 presents high MDR rainfall, twice higher than NCEP-2. NCEP-2 is in the middle of the points of the models while ERA-40 is off-centered. MRI, IAP and CSIRO0 have low

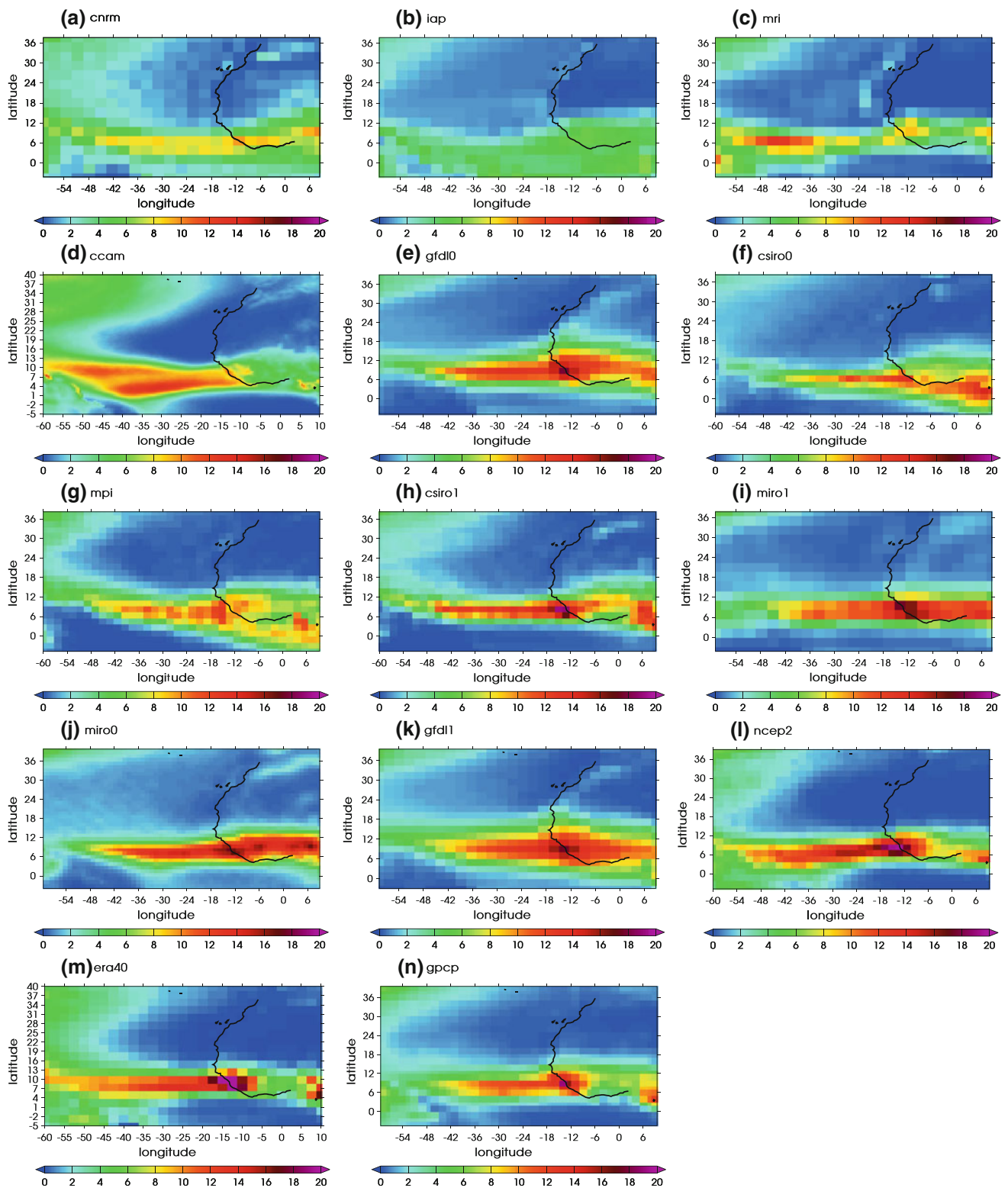


**Fig. 4** As in Fig. 3, except for total precipitation ( $\text{mm day}^{-1}$ ), and n) for GPCP

to moderate AEW activity and low MDR rainfall, but MRI and IAP do not produce TCs whereas CSIRO0 does. Similarly, CNRM, CCAM and GFDL0 have moderate AEW activity and MDR rainfall, however CNRM and

CCAM are not producing TCs in the MDR while GFDL0 does. This shows that it is not possible to establish a strong relationship between TC activity and MDR rainfall in these models, even when adding the influence of AEW activity.

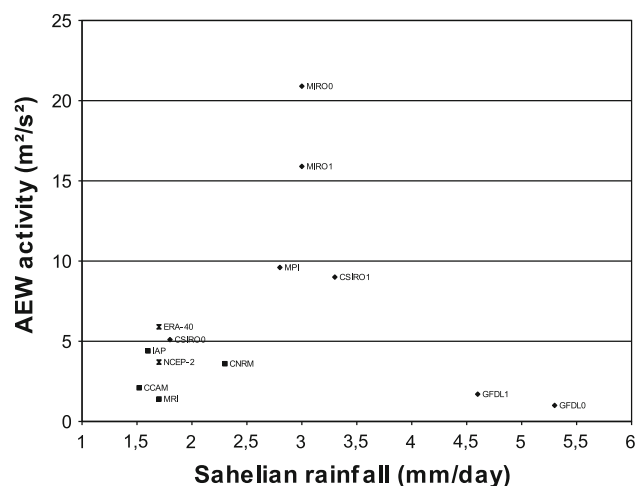


**Fig. 5** Scatter plot of AEW activity ( $\text{m}^2 \text{s}^{-2}$ ) versus Sahelian rainfall ( $\text{mm day}^{-1}$ ) for JAS 1980–1998. *Diamonds* represent simulations producing TCs, *squares* those not producing TCs and *doubles triangles* represent reanalyses

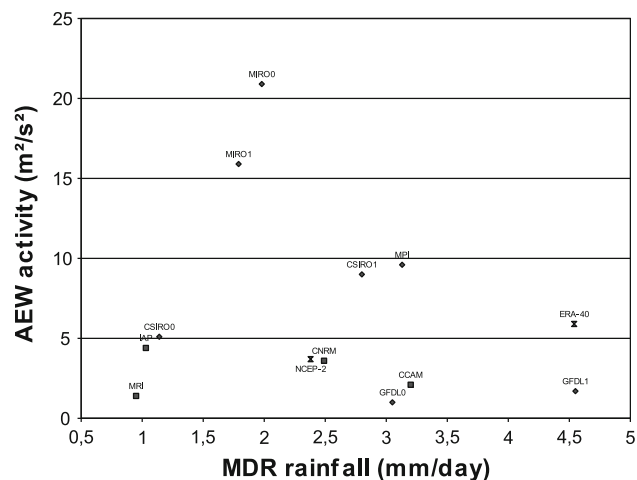


**Fig. 6** As in Fig. 5, except for AEW activity ( $\text{m}^2 \text{s}^{-2}$ ) versus MDR rainfall ( $\text{mm day}^{-1}$ )

However when FD rainfall is considered (Fig. 7) it is found to correlate well with AEW activity and may be a good indicator of TCs over the MDR. For FD rainfall, ERA-40 and NCEP-2 show closer locations on the scatter plot, compared to the one for the MDR rainfall (cf. Fig. 6). They are both off-centered compared to the models. As discussed by Berry and Thorncroft (2005), the merger of potential vorticity (PV) anomalies that are generated by convection over these highlands can result in the production of a significant PV feature that leaves the West African coast and rapidly undergoes tropical cyclogenesis. This relationship between FD rainfall and TC activity over the MDR does not exist for all models e.g. GFDL0 and GFDL1. This is most likely due to the fact that the large amount of rainfall

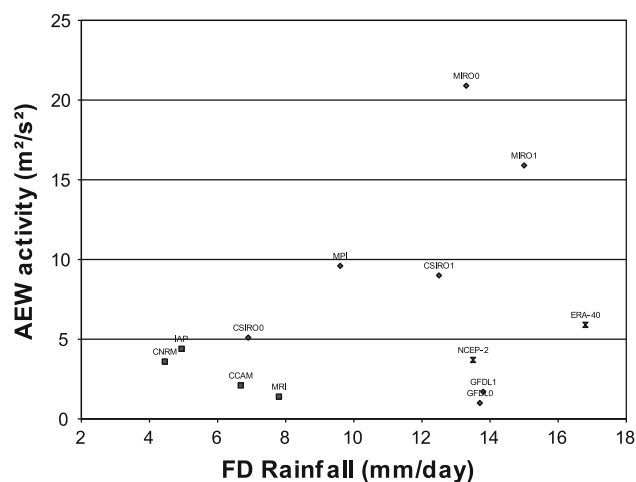


**Fig. 7** As in Fig. 5, except for AEW activity ( $\text{m}^2 \text{s}^{-2}$ ) versus the Fouta Djallon rainfall ( $\text{mm day}^{-1}$ )

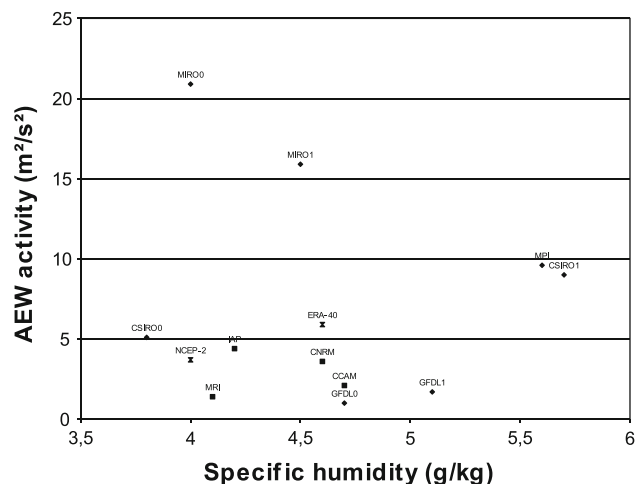


**Fig. 8** As in Fig. 5, except for AEW activity ( $\text{m}^2 \text{s}^{-2}$ ) versus specific humidity ( $\text{g/kg}$ ) at 600 hPa for 5–15°N, 15–30°W

over Africa in those models is not associated with propagating AEWs and is thus not influencing TC genesis.

The influence of mid-tropospheric (600 hPa) specific humidity over the ocean is now examined (Fig. 8). ERA-40 and NCEP-2 present distinct locations due to their difference in specific humidity. ERA-40 is located in the middle of all the models while NCEP-2 is isolated due to its low specific humidity. GFDL0 and GFDL1 have low AEW activity but moderate to high values of specific humidity which may explain the development of TCs in these models. In contrast, CSIRO0 has intense AEW activity, but a very low specific humidity over the ocean, which could explain its low TC activity. Tropospheric humidity over the ocean does not explain the non development of TCs in the

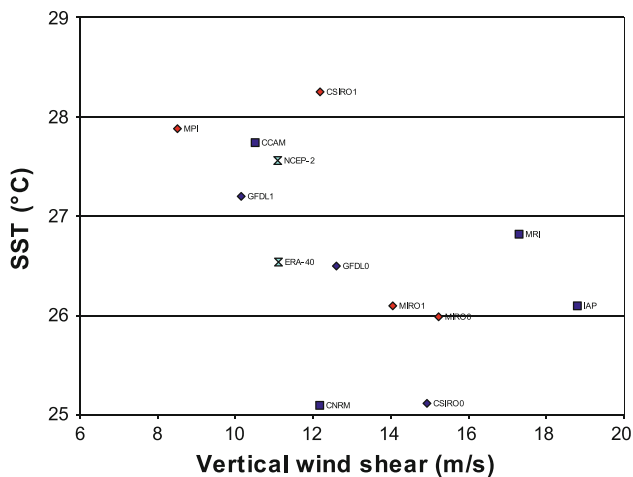


**Fig. 9** As in Fig. 5, except for SST ( $^{\circ}\text{C}$ ) versus wind shear ( $\text{m s}^{-1}$ ) between 850 and 200 hPa. Red (resp. dark blue) points denote simulations with a high (resp. low to moderate) AEW activity. Light blue double triangles represent reanalyses

CNRM, IAP and MRI models so other features must be responsible for their low TC activity.

A scatter plot linking the vertical wind shear and SST values averaged over the MDR for all the models and reanalyses is shown in Fig. 8. The models producing TCs have large variations in their combination of SST, wind shear and AEW activity. For instance, CSIRO1 and MPI produce TCs and have high AEW activity (meridional wind variance of about  $9 \text{ m}^2 \text{ s}^{-2}$ ), warm SST (above  $27^{\circ}\text{C}$ ), and low to moderate vertical wind shear (between  $8$  and  $12 \text{ m s}^{-1}$ ). GFDL1 which also produces TCs, has warm SST ( $27.2^{\circ}\text{C}$ ) and low wind shear ( $10.5 \text{ m s}^{-1}$ ), but low AEW activity ( $1.7 \text{ m}^2 \text{ s}^{-2}$ ). MIRO0 and MIRO1 produce TC and have very high AEW activity (over  $16 \text{ m}^2 \text{ s}^{-2}$ ) with moderate SST (about  $25.5^{\circ}\text{C}$ ) and moderate to high wind shear (about  $15 \text{ m s}^{-1}$ ). CSIRO0 has a moderate AEW activity ( $5 \text{ m}^2 \text{ s}^{-2}$ ), relatively cold SST ( $25.1^{\circ}\text{C}$ ) and substantial vertical wind shear ( $15.1 \text{ m s}^{-1}$ ). GFDL0 has very low AEW activity ( $1 \text{ m}^2 \text{ s}^{-2}$ ) with moderate wind shear ( $12.6 \text{ m s}^{-1}$ ) and warm SST ( $26^{\circ}\text{C}$ ). To examine the environmental fields influencing tropical cyclogenesis in more detail, the TC genesis indices described in Sect. 2 will now be analysed and compared with the detected TCs.

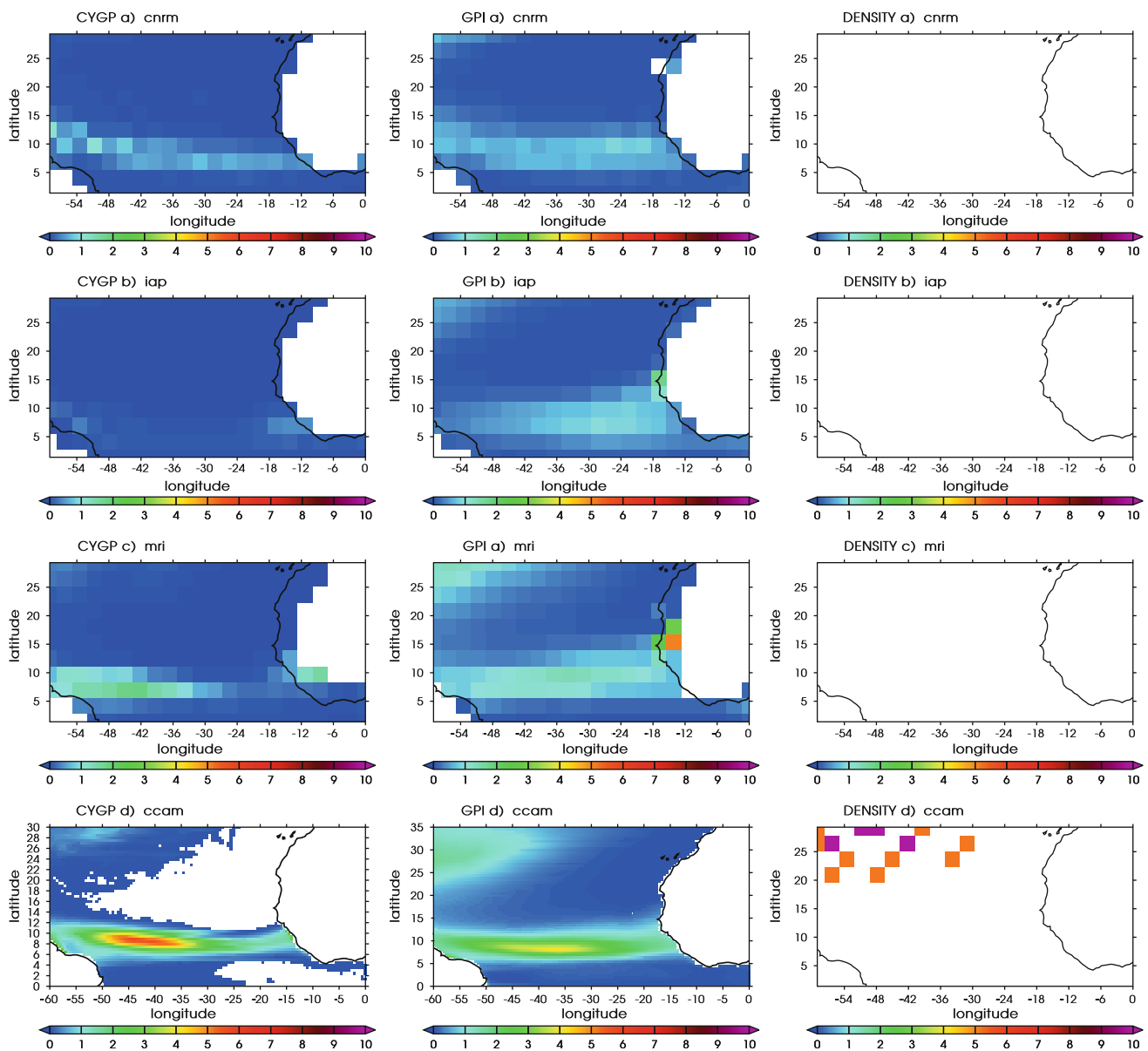
## 5 Comparison between TC genesis indices and detected cyclogenesis

Figure 10 shows CYGP, GPI and the density of detected points of TC genesis for the models with the lowest number of detected TCs in the MDR (see Table 2). The only detected TCs for CCAM are from tracks recurving eastward from the Gulf of Mexico and the western tropical Atlantic, so they are not taken into account for the TC

activity over the MDR. The first and second columns of Fig. 10 clearly show similarities between CYGP and GPI for these four simulations. Except for IAP, values of CYGP and GPI between 1 and 7 TCs per 20 years per  $5^{\circ}$  by  $5^{\circ}$  boxes are found in a band following the ITCZ (between  $60^{\circ}\text{W}$  and  $10^{\circ}\text{W}$ ). For IAP, this is true for the GPI but not for the CYGP that is close to 0. This may be explained by the very low rainfall over Africa and the Atlantic in this model (Fig. 4b) and hence values of convective precipitation which drive the CYGP will also be low. IAP also has the strongest wind shear among all the models analysed, implying that the dynamic part of both indices is less favourable for cyclogenesis than in other models. In the MRI model, CYGP is very low in the eastern part of the Atlantic while larger values are found between  $60^{\circ}\text{W}$  and  $30^{\circ}\text{W}$ . This region of low CYGP may explain the low rate of cyclogenesis in the MDR for this model. Thus, Fig. 10 shows that there is a good correspondence between the lack of cyclogenesis and low values of both indices.

Figure 11 is the same as Fig. 10 but for models with moderate TC activity over the MDR. Both genesis indices have values of approximately 3 TCs per 20 year per  $5^{\circ}$  by  $5^{\circ}$  boxes over the MDR, averaged over JAS 1980–1998. For all models, with the exception of MPI, genesis maxima follow a continuous belt between  $10^{\circ}\text{W}$  and  $50^{\circ}\text{W}$ . Like MRI (Fig. 10), MPI shows a maximum for both indices between  $30^{\circ}\text{W}$  and  $60^{\circ}\text{W}$  which may explain the low rate of cyclogenesis over the eastern Atlantic. CSIRO0, MPI and CSIRO1 show a good correspondence between indices and cyclogenesis over the MDR, while GFDL0 does not. GFDL0 is interesting since the amplitude of both indices is high whereas cyclogenesis is rare. This may be associated with the lack of AEWs produced in this model. GFDL0 is an interesting case since it displays all the conditions for TC genesis, including a large rainfall rate over the Sahel and FD regions, with the exception of producing AEWs.

CYGP, GPI and the density of TC genesis detected for the models with the highest TC activity are shown in Fig. 12. The genesis indices for these models reach maximum values of approximately 3 TCs per 20 years per  $5^{\circ}$  by  $5^{\circ}$  boxes over the MDR, averaged over JAS 1980–1998. MIRO1 shows a good correlation between the genesis indices and cyclogenesis whereas MIRO0 and GFDL1 do not. MIRO0 is particularly active over the eastern Atlantic with cyclogenesis rate reaching more than 8 TCs over some  $5^{\circ} \times 5^{\circ}$  boxes. MIRO0 and MIRO1 are two of the models that produce the most rainfall over the Fouta Djallon highlands (Fig. 4), suggesting that rainfall in this region is a good precursor of cyclogenesis. The density of TCs simulated in these models is surprising since SST and wind shear over the MDR are not favourable for cyclogenesis, leading to low genesis indices. TC activity in MIRO0 and MIRO1 appears to be governed by their high AEW activity



**Fig. 10** CYGP (left column), GPI (middle column), and density of TC genesis per 20 years per  $5^\circ$  by  $5^\circ$  boxes (right column) for simulations with low TC activity: **a** CNRM, **b** IAP, **c** MRI and **d** CCAM

whilst the low AEW activity in GFDL1 is balanced by a very large rainfall rate, so that this model is able to produce some TCs. Sall et al. (2006) and Arnault and Roux (2011) showed that humidity over the eastern tropical Atlantic is also an important factor to understand why some waves develop as TCs while others do not.

## 6 Conclusion and discussion

In this paper, we investigated the ability of GCMs to simulate the TC activity over the North Atlantic MDR and the factors influencing this ability. The selected GCMs are coupled

ocean–atmosphere models from the TC-MIP archive, a subset of the CMIP-3 archive with a horizontal resolution from  $1^\circ$  to  $2.8^\circ$ , and CCAM a high horizontal resolution ( $0.5^\circ$ ) atmospheric model forced by bias-corrected SSTs. In Sect. 3, we showed that strong biases are present over the MDR in terms of production of TCs. Some models (CNRM, IAP, MRI and CCAM) do not simulate any TCs over this region.

Models have large deficiencies when simulating TC activity and the numbers of TCs are low in comparison with observations. Even with the use of the resolution-dependent wind speed threshold of Walsh et al. (2007), the detection of the TCs in models is highly variable. The biases revealed in Sect. 3 are partly due to the low temporal

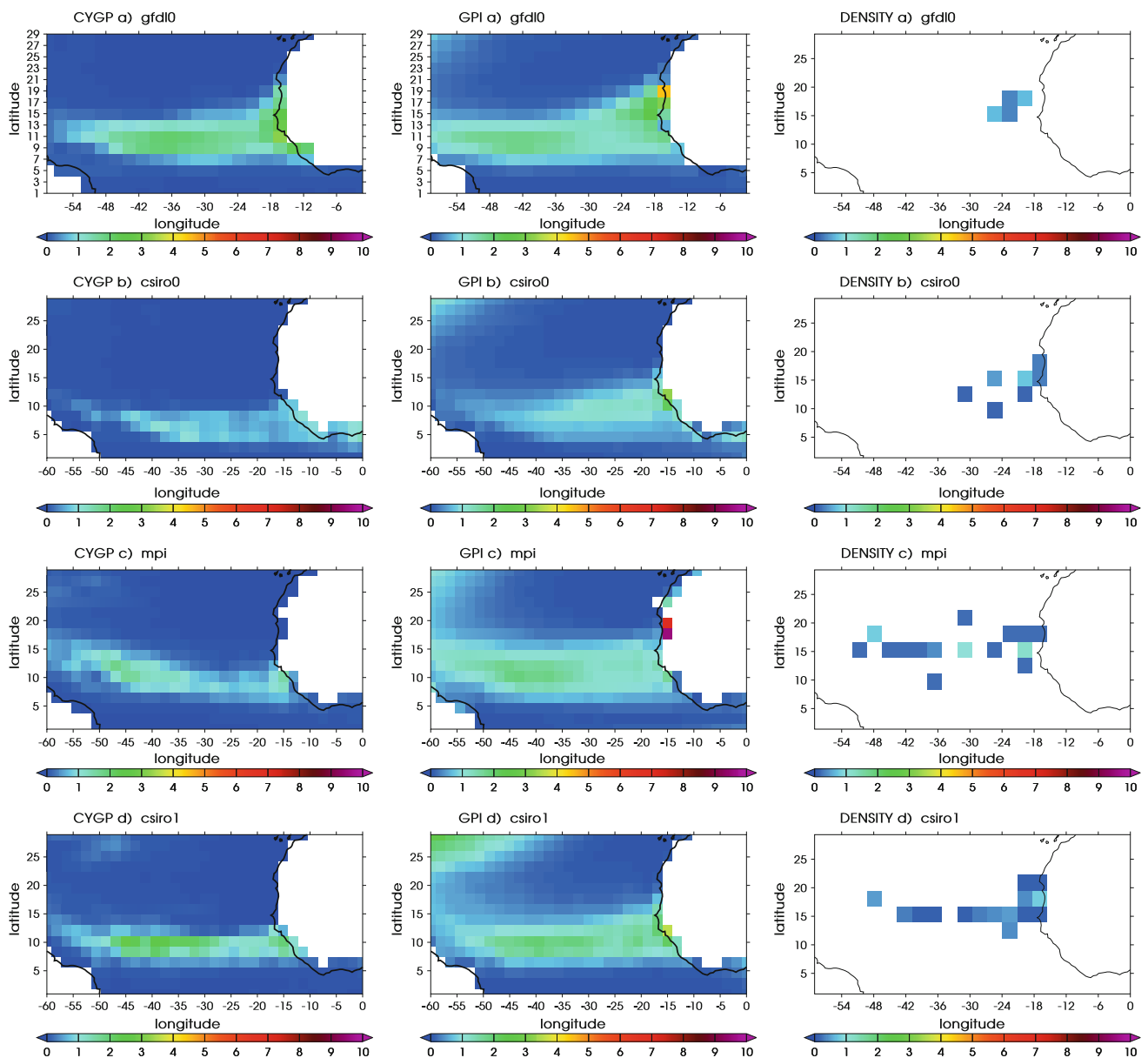


**Fig. 11** As in Fig. 10, except for simulations with moderate AEW activity: **a** GFDL0, **b** CSIRO0, **c** MPI and **d** CSIRO1. All these models have a moderate TC activity (cf. Table 2).

and spatial resolutions of the TCMIP models. All models underestimate TCs in the western MDR and in the western Atlantic basin, even when TC activity in the overall MDR is correctly represented. As a conclusion one may infer that TCMIP models do not have fine enough resolution to allow realistic development of TCs. However, the ability of models to simulate TCs is not only linked to resolution since the relatively high-resolution CCAM model does not produce TCs over the MDR, even when employing a lower wind speed threshold. Overall, it is clear from this study that TCs in the MDR result from a combination of processes and the models all differ in their representation of these processes.

The majority of models that simulate TCs in the MDR (MIRO1, CSIRO1, MPI and CSIRO0) are overestimating the AEW activity by up to 3 times that shown in the NCEP-2 and ERA-40 reanalyses. This result suggests that AEW activity is a controlling factor in the ability of models to simulate TCs in the MDR. However, GFDL1 has a low AEW activity but produces TCs, showing that other factors are important for TC genesis in the MSR. All models with high AEW activity and/or precipitation over the Fouta Djallon highlands (GFDL0, CSIRO0, MPI, CSIRO1, MIRO1, MIRO0 and GFDL1) simulate TCs. The importance of rainfall over the Fouta Djallon highlands combined with AEW activity to discriminate between the

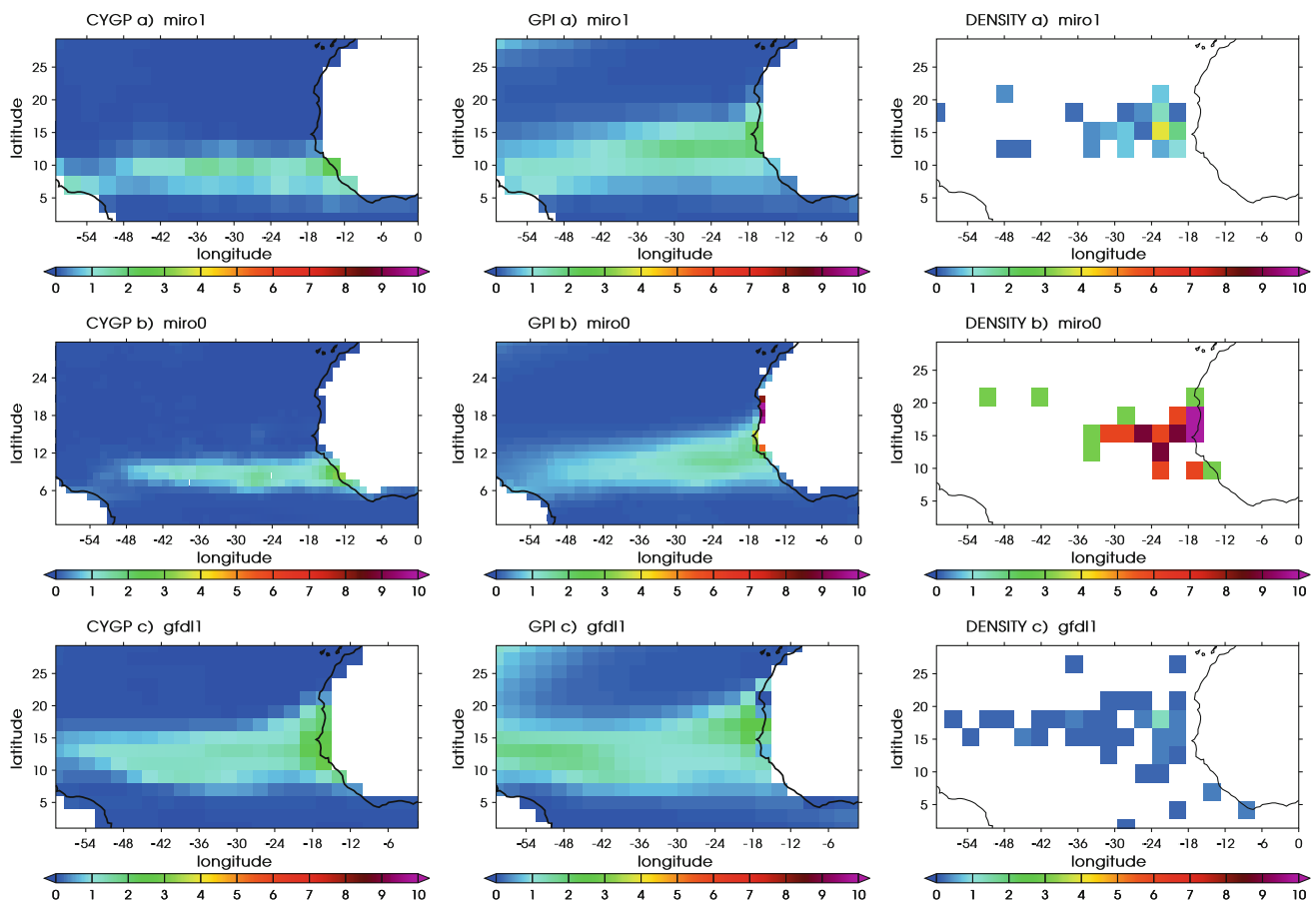


**Fig. 12** As in Fig. 10, except for simulations with high AEW activity: **a** MIRO1, **b** MIRO0 and **c** GFDL1

model formation rates of TCs over the MDR has been emphasized in this study.

Reaching a threshold in SST and/or vertical wind shear is a necessary condition for tropical cyclogenesis in models, however it does not necessarily imply TC genesis. For example, CCAM has warm SST and low wind shear, but does not produce TCs. The low values of AEW activity and rainfall over Fouta Djallon can explain the lack of cyclogenesis in the MDR in this model. These variables are all important for tropical cyclogenesis but the fact that a model may display one or many of these factors does not mean the model will necessarily simulate a realistic number of TCs in the MDR. The resulting TCs are a combination of some of these conditions, with the most important factors influencing TC genesis varying from one model to another.

In Sect. 5, we examined the ability of two TC genesis indices, CYGP and GPI, to represent TC genesis over the MDR in TCMIP and CCAM simulations. Models which do not produce TCs show low CYGP and GPI indices over the MDR and eastern tropical Atlantic (Fig. 10). These models (CNRM, IAP and MRI) also have strong negative biases in rainfall over these regions (Fig. 4), suggesting that rainfall is a crucial ingredient for TC genesis. In the CYGP, using

convective precipitation, Royer et al. (1998) integrates the static stability, the humidity and the vertical movements of the atmosphere. Rainfall can indeed be considered as a potential for TC formation and not only a trigger. For this reason, CYGP seems to be more accurate than GPI to represent cyclogenesis over eastern Atlantic, even though GPI takes into account potential intensity and relative humidity which are also related to rainfall. For the models producing larger number of TCs, the relationship is less evident, but the genesis indices show some success in representing tropical cyclogenesis. The use of tropical cyclogenesis indices is shown to be a fairly reliable way to assess TC genesis, although the relationship is not always obvious. To improve the genesis indices, a number of other factors should be considered. Previous studies have shown that the large scale fields do not impact TC genesis in the same way in all basins (Gualdi et al. 2008). However, the large-scale fields used in the indices do not take in account the specific characteristics of each basin. Also, the meso and small scale processes associated with genesis are not exactly the same in all basins. The results presented here show that rainfall over the Sahel and mid-tropospheric humidity may be as important factors for TC genesis as



AEW activity is in the MDR. These phenomena should therefore be taken in account when analysing the simulation of TCs in the MDR. This point certainly deserves further investigations.

**Acknowledgments** We acknowledge the modelling groups, the Program for Climate Model Diagnosis and Intercomparison (PCMDI) and the WCRP's Working Group on Coupled Modelling (WGCM) for their roles in making available the WCRP CMIP3 multi-model dataset. Support for this dataset is provided by the Office of Science, US Department of Energy. We also acknowledge the University of Toulouse for partly financing the project.

## References

- Arnault J, Roux F (2011) Characteristics of African Easterly waves associated with tropical cyclogenesis in the Cape Verde Islands region in July–August–September of 2004–2008. *Atmos Res* 100:61–82
- Bengtsson L, Bottger H, Kanamitsu M (1982) Simulation of hurricane-type vortices in a general circulation model. *Tellus* 34:440–457
- Bengtsson L, Botzet M, Esch M (1996) Will greenhouse gas-induced warming over the next 50 years lead to higher frequency and greater intensity of hurricanes? *Tellus* 48:57–73
- Bengtsson L, Hodges KH, Esch M, Keenlyside N, Kornbluh L, Luo J–J, Yamagata T (2007) How may tropical cyclones change in a warmer climate? *Tellus* 59:539–561
- Berry GJ, Thorncroft C (2005) Case study of an intense African Easterly Wave. *Mon Weather Rev* 133:752–766
- Bister M, Emanuel KA (1998) Dissipative heating and hurricane intensity. *Meteor Atmos Phys* 65:233–240
- Braun SA (2010) Reevaluating the role of Saharan air layer in Atlantic tropical cyclogenesis and evolution. *Mon Wea Rev* 138. doi:10.1175/2009MWR3135.1
- Broccoli A, Manabe S (1990) Can existing climate models be used to study anthropogenic changes in tropical cyclone climate? *Geophys Res Lett* 17:1917–1920
- Burpee RW (1972) The origin and structure of easterly waves in the lower troposphere of North Africa. *J Atmos Sci* 29:77–90
- Burpee RW (1974) Characteristics of North African easterly waves during the summers of 1968 and 1969. *J Atmos Sci* 31:1556–1570
- Camargo SJ, Barnston AG, Zebiak SE (2005) A statistical assessment of tropical cyclone activity in atmospheric general circulation models. *Tellus* 57A:589–604
- Camargo SJ, Emanuel KA, Sobel AH (2007) Use of a genesis potential index to diagnose ENSO effects on tropical cyclone genesis. *J Clim* 20:4819–4834
- Carlson TN (1969) Some remarks on African disturbances and their progress over the tropical Atlantic. *Mon Weather Rev* 97:716–726
- Caron LP, Jones CG, Winger K (2010) Impact of resolution and downscaling technique in simulating recent Atlantic tropical cyclone activity. *Clim Dyn*. doi:10.1007/s00382-010-0846-7
- Chauvin F, Royer JF, Déqué M (2006) Response of Hurricane-type vortices to global warming as simulated by the ARPEGE-Climat at high resolution. *Clim Dyn* 27:377–399
- Chen SS, Knaff JA, Marks Jr FD (2006) Effects of vertical wind shear and storm motion on tropical cyclone rainfall asymmetries deduced from TRMM. *Mon Weather Rev* 134:3190–3208
- Delworth TL et al (2006) GFDL's CM2 global coupled climate models. Part I: formulation and simulation characteristics. *J Clim* 19:643–674
- Dunion JP, Velden CS (2004) The impact of the Saharan air layer on Atlantic tropical cyclone activity. *Bull Am Meteor Soc* 85:353–365
- Emanuel KA, Nolan D (2004) Tropical cyclone activity and the global climate system. Preprints of the 26th conference on hurricane and tropical meteorological. Am Meteor Soc, Miami Beach, FL, USA, 3–7 May 2004
- Fink AH, Schrage JM, Kotthaus S (2010) On the potential causes of the nonstationary correlations between West African precipitation and Atlantic hurricane activity. *J Clim* 23:5437–5456
- Fyfe JC (1999) Climate simulations of African Easterly Waves. *J Clim* 12:1747–1769
- Garner ST, Held IM, Knuston T, Sirutis J (2009) The roles of wind shear and thermal stratification in past and projected changes of Atlantic tropical cyclone activity. *J Clim* 22:4723–4734
- Goldenberg SB, Shapiro LJ (1996) Physical mechanisms for the association of El Niño and the West African rainfall with Atlantic major hurricane variability. *J Clim* 9:1169–1187
- Gray WM (1968) Global view of the origin of tropical disturbances and storms. *Mon Weather Rev* 96:669–700
- Gray WM (1975) Tropical cyclone genesis. Department of Atmospheric Science paper, No. 234, Colorado State University, Fort Collins, Co, 21 p
- Gray WM (1990) Strong association between West African rainfall and US landfalling intense hurricanes. *Science* 249:1251–1256
- Gualdi S, Scoccimarro E, Navarra A (2008) Changes in tropical cyclone Activity due to global warming: results from a high-resolution coupled general circulation model. *J Clim* 21:5204–5228
- Haarsma R, Mitchell J, Senior C (1993) Tropical disturbances in a GCM. *Clim Dyn* 8:247–257
- Hopsch SB, Thorncroft CD, Hodges K, Ayyer A (2007) West African storm tracks and their relationship to Atlantic tropical cyclones. *J Clim* 20:2468–2483
- Hopsch SB, Thorncroft CD, Tyle KR (2010) Analysis of African Easterly waves structures and their role in influencing tropical cyclogenesis. *Mon Weather Rev* 138:1399–1419
- Hsieh J-S, Cook KH (2007) A study of the energetics of African Easterly waves using a regional climate model. *J Atmos Sci* 64:421–440
- Huffman G, Adler R, Morrissey M, Bolvin D, Curtis S, Joyce R, McGavock B, Susskind J (2001) Global precipitation at one-degree daily resolution from multi-satellite observations. *J Hydrometeor* 2:36–50
- Kanamitsu M, Ebisuzaki W, Woollen J, Yang S-K, Hnilo JJ, Fiorino M, Potter GL (2002) NCEP-DOE AMIP-II reanalysis. *Bull Am Meteorol Soc*. doi:10.1175/BAMS-83-11-1631
- Klotzbach PJ, Gray WM (2004) Updated 6–11 month prediction of Atlantic basin seasonal hurricane activity. *Wea Forecast* 19:917–934
- Knapp KR, Kruk MC, Levinson DH, Diamond HJ, Neumann CJ (2010) The international best track archive for climate stewardship (IBTrACS): unifying tropical cyclone best track data. *Bull Am Meteor Soc* 91:363–376
- Krishnamurti TN, Oosterhof DK, Dignon N (1989) Hurricane prediction with a high resolution global model. *Mon Weather Rev* 117:631–669
- Landsea CW (1993) A climatology of intense (and major) Atlantic hurricanes. *Mon Weather Rev* 121:1703–1713
- Landsea CW, Gray W (1992) The strong association between Western Sahelian monsoon rainfall and intense Atlantic hurricanes. *J Clim* 5:435–453
- Manabe S, Holloway JL, Stone H (1970) Tropical circulation in a time-integration of a global model of the atmosphere. *J Atmos Sci* 27:580–613
- McDonald RE, Bleaken DG, Cresswell DR, Pope VD, Senior CA (2005) Tropical storms: representation and diagnosis in climate models and the impacts of climate change. *Tellus* 25:19–36

- McGregor JL, Dix MR (2001) The CSIRO conformal-cubic atmospheric GCM. In: Hodnett PF (ed) IUTAM symposium on advances in mathematical modelling of atmosphere and ocean dynamics. Kluwer, Dordrecht, pp 197–202
- Meehl GA, Stocker TF, Collins WD, Friedlingstein P, Gaye AT, Gregory JM, Kitoh A, Knutti R, Murphy JM, Noda A, Raper SCB, Watterson IG, Weaver AJ, Zhao Z-C (2007) Global climate projection. In: Solomon S, Qin D, Manning M, Chen Z, Marquis M, Averyt KB, Tignor M, Miller HL (eds) *Climate change 2007: the physical science basis*. Contribution of working group I to the fourth assessment report of the intergovernmental panel on climate change. Cambridge University Press, Cambridge, UK and New York, NY, USA
- Montgomery MJ (2011) The PRE-depression investigation of cloud-systems in the tropics (PREDIC) experiment: scientific basis and some first results. *Bull Am Meteor Soc* (in review)
- Neumann CJ, Jarvinen BR, McAdie CJ, Hammer GR (1999) Tropical cyclones of the North Atlantic Ocean, 1871–1999. NOAA/NWS/NESDIS, *Historical Climatology Series* 6-2, p 206
- Oouchi K, Yoshimura J, Yoshimura H, Mizuta R, Kusunoki S, Noda A (2006) Tropical cyclone climatology in a global-warming climate as simulated in a 20 km-mesh global atmospheric model: frequency and wind intensity analyses. *J Meteor Soc Japan* 84:259–276
- Redelsperger J-L, Thorncroft CD, Diedhiou A, Lebel T, Parker D, Polcher J (2006) African monsoon multidisciplinary analysis (AMMA)–international research project and field campaign. *Bull Am Meteor Soc* 87(12):1739–1746
- Reed RJ, Norquist DC, Recker EE (1977) The structure and properties of African wave disturbances as observed during phase III of GATE. *Mon Weather Rev* 105:317–333
- Reed RJ, Hollingsworth A, Heckley WA, Delsol F (1988) An evaluation of the performance of the ECMWF operational system in analyzing and forecasting easterly wave disturbances over Africa and the tropical Atlantic. *Mon Weather Rev* 116:824–865
- Royer J-F, Chauvin F (2009) Response of tropical cyclogenesis to global warming in an IPCC AR-4 scenario assessed by a modified yearly genesis parameter. In: Elsner JB, Jagger TH (eds) *Hurricanes and climate change*. Springer, Berlin, pp 213–234
- Royer J-F, Chauvin F, Timbal B, Araspin P, Grimal D (1998) A GCM study of the impact of greenhouse gas increase on the frequency of occurrence of tropical cyclones. *Clim Change* 38:307–347
- Ruti PM, Dell'Aquila A (2010) The twentieth century African Easterly Waves in reanalysis systems and IPCC simulations, from intra-seasonal to inter-annual variability. *Clim Dyn* 35:1099–1117
- Sall SM, Sauvageot H, Gaye AT, Viltard A, Felice P (2006) A cyclogenesis index for tropical Atlantic off the African coasts. *Atmos Res* 79:123–147
- Sud YC, Walker GK, Lau K-M (1999) Mechanisms regulating sea-surface temperatures and deep convection in the tropics. *Geophys Res Lett* 26:1019–1022
- Sugi MA, Noda A, Sato N (2002) Influence of the global warming on tropical cyclone climatology: an experiment with the JMA global model. *J Meteor Soc Japan* 80:249–272
- Thompson RM, Payne SW, Recker EE, Reed RJ (1979) Structure and properties of the synoptic-scale wave disturbances in the intertropical convergence zone of the eastern Atlantic. *J Atmos Sci* 36:53–72
- Thorncroft CD, Hodges K (2001) African Easterly wave variability and its relationship to Atlantic tropical cyclone activity. *J Clim* 14:1166–1179
- Thorncroft CD, Hoskins BJ (1994) An idealized study of African easterly waves. I: a linear view. *Quart J Roy Meteor Soc* 120:953–982
- Uppala SM, Kallberg PW, Simmons UA, Andrae J, Bechtold VD, Fiorino M, Gibson JK, Haseler J, Hernandez A, Kelly GA, Li X, Onogi K, Saarinen S, Sokka N, Allan RP, Andersson E, Arpe K, Balmaseda MA, Beljaars ACM, Van De Berg L, Bidlot J, Bormann N, Caires S, Chevallier F, Dethof A, Dragosavac M, Fisher M, Fuentes M, Hagemann S, Holm E, Hoskins BJ, Isaksen I, Janssen PAEM, Jenne R, McNally AP, Mahfouf JF, Morcrette JJ, Rayner NA, Saunders RW, Simon P, Sterl A, Trenberth KE, Untch A, Vasiljevic D, Viterbo P, Woollen J (2005) The ERA-40 re-analysis. *Quart J Roy Meteor Soc* 131:2961–3012
- Vecchi GA, Soden BJ (2007) Increased tropical Atlantic wind shear in model projections of global warming. *Geophys Res Lett* 34:L08702
- Walsh KJE, Watterson IG (1997) Tropical Cyclone-like vortices in a limited area model: Comparison with observed climatology. *J Clim* 10:2240–2259
- Walsh KJE, Nguyen K-C, McGregor JL (2004) Fine-resolution regional climate model simulations of the impact of climate change on tropical cyclones near Australia. *Clim Dyn* 22:47–56
- Walsh KJE, Fiorino M, Landsea CW, McInnes KL (2007) Objectively determined resolution-dependent threshold criteria for the detection of tropical cyclones in climate models and reanalysis. *J Clim* 20:2307–2314
- Walsh KJE, Lavender S, Murakami H, Scoccimarro E, Caron L-P, Gantous M (2010) The tropical cyclone climate model inter-comparison project. In: Elsner JB, Jagger TH (eds) *Hurricanes and climate change*, vol 2. Springer, Berlin, pp 1–24